Characterization of the Interaction between Manganese and Tyrosine Z in Acetate-Inhibited Photosystem II†

Veronika A. Szalai,‡ Henriette Kühne,§ K. V. Lakshmi,‡ and Gary W. Brudvig*,‡

Department of Chemistry and Department of Molecular Biophysics and Biochemistry, Yale University, New Haven, Connecticut 06520

Received June 1, 1998; Revised Manuscript Received July 28, 1998

ABSTRACT: When acetate-inhibited photosystem II (PSII) membranes are illuminated at temperatures above 250 K and quickly cooled to 77 K, a 240 G-wide electron paramagnetic resonance (EPR) signal is observed at 10 K. This EPR signal arises from a reciprocal interaction between the spin $^1/_2$ ground state of the S_2 state of the Mn_4 cluster, for which a multiline EPR signal with shifted ^{55}Mn hyperfine peaks is observed, and the oxidized tyrosine residue, $Y_Z^\bullet$, for which a broadened $Y_Z^\bullet$ EPR spectrum is observed. The $S_2Y_Z^\bullet$ EPR signal in acetate-inhibited PSII is the first in which characteristic spectral features from both paramagnets can be observed. The observation of distinct EPR signals from each of the paramagnets together with the lack of a half-field EPR transition indicates that the exchange and dipolar couplings are weak. Below 20 K, the $S_2Y_Z^\bullet$ EPR signal in acetate-inhibited PSII is in the static limit. Above 20 K, the line width narrows dramatically as the broad low-temperature $S_2Y_Z^\bullet$ EPR signal is converted to a narrow $Y_Z^\bullet$ EPR signal at room temperature. The line width narrowing is interpreted to be due to averaging of the exchange and dipolar interactions between $Y_Z^\bullet$ and the S_2 state of the Mn_4 cluster by rapid spin−lattice relaxation of the Mn_4 cluster as the temperature is increased. Decay of the $S_2Y_Z^\bullet$ intermediate at 200 K shows that the $g = 4.1$ form of the S_2 state is formed and that a noninteracting S_2-state multiline EPR signal is not observed as an intermediate in the decay. This result shows that a change in the redox state of Y_Z induces a spin-state change in the Mn_4 cluster in acetate-inhibited PSII. The interconversion between spin states of the Mn_4 cluster in acetate-inhibited PSII supports the idea that Y_Z oxidation or $Y_Z^\bullet$ reduction is communicated to the Mn_4 cluster through a direct hydrogen-bonding pathway, possibly involving a ligand bound to the Mn_4 cluster.

In green plants, light-driven oxidation of water to dioxygen and reduction of plastoquinone to plastoquinol are carried out by the membrane-bound protein complex photosystem II (PSII)[1] (*1*−*3*). To produce dioxygen, the O_2-evolving complex (OEC), containing a tetranuclear manganese−oxo cluster, is oxidized in four photochemical steps and cycles through five "store" or S states labeled S_0−S_4 (*4*). On the basis of X-ray absorption measurements of the dark-stable S_1 state, the Mn_4 cluster has been modeled as an unsymmetrical dimer of dimers (*5*), although the structure of the Mn_4 cluster is still under debate. The S_2 state is an odd-electron state, and electron paramagnetic resonance (EPR) spectroscopy has been used extensively to study the Mn_4 cluster in the S_2 state [reviewed in Miller and Brudvig (*6*)].

The physiological oxidant of the Mn_4 cluster is a redox-active tyrosine known as Y_Z (*7*, *8*). In O_2-evolving PSII membranes, oxidized Y_Z is difficult to observe by EPR spectroscopy because its re-reduction by the Mn_4 cluster is extremely rapid. However, time-resolved EPR has been used to observe $Y_Z^\bullet$ at room temperature in O_2-evolving PSII samples (*9*, *10*). $Y_Z^\bullet$ can also be trapped by freezing a Mn-depleted PSII sample under illumination (*11*). In both samples, $Y_Z^\bullet$ exhibits an EPR signal less than 30 G wide that is similar to the EPR signal of the dark-stable tyrosine radical in PSII, $Y_D^\bullet$. Several chemical treatments, including depletion of calcium or chloride or addition of acetate, ammonia, or fluoride, block the S-state cycle and cause a shutdown of the water oxidation chemistry at the S_2 state. These inhibitory treatments may perturb the binding of substrate water or displace chloride or calcium ions required for maximal O_2 evolution. When such inhibited PSII samples are continuously illuminated at temperatures above 250 K and then quickly cooled to 77 K, an EPR signal greater than 100 G wide and centered at $g = 2$ can be observed at 10 K (*12*−*20*). This signal, previously referred to as the S3 EPR signal, has been identified as arising from the interaction of $Y_Z^\bullet$ (*21*, *22*) with the S_2 state of the Mn_4 cluster in acetate-inhibited PSII samples (*23*). However, during steady-state illumination at room temperature, a narrow $Y_Z^\bullet$ EPR signal, similar to that observed in Mn-depleted PSII samples, has

† Supported by the National Institutes of Health (Grants GM 32715 and GM 36442) and by a National Institutes of Health predoctoral traineeship to V.A.S. (GM 08283).

* To whom correspondence should be addressed. Telephone: (203) 432-5202. Fax: (203) 432-6144. E-mail: Gary.Brudvig@yale.edu.

‡ Department of Chemistry.

§ Department of Molecular Biophysics and Biochemistry.

[1] Abbreviations: chl, chlorophyll; DCMU, 3-(3,4-dichlorophenyl)-1,1-dimethylurea; DMSO, dimethyl sulfoxide; EGTA, ethylene glycol bis(β-aminoethyl ether)-*N*,*N*,*N*′,*N*′-tetraacetic acid; EPR, electron paramagnetic resonance; MES, 2-morpholinoethanesulfonic acid; NO•, nitric oxide; OEC, O_2-evolving complex; PPBQ, phenyl-*p*-benzoquinone; PSII, photosystem II; Y_D, tyrosine 160 of the D2 polypeptide; Y_Z, tyrosine 161 of the D1 polypeptide.

S0006-2960(98)01302-6 CCC: $15.00
Published on Web 09/05/1998

been observed from ammonia-inhibited (*24*) or calcium-depleted PSII (*25*, *26*). As in untreated PSII (*27*), the $Y_Z^•$ EPR signal induced in ammonia-inhibited PSII (*24*) saturates at a much higher microwave power than in a Mn-depleted PSII sample, indicating that the spin relaxation of $Y_Z^•$ is enhanced by its proximity to the Mn_4 cluster. Because of the different EPR properties of $Y_Z^•$ at cryogenic and room temperatures, it is unclear whether the same $S_2Y_Z^•$ state is being observed at all temperatures. To differentiate the low-temperature S3 EPR signal from the narrow $Y_Z^•$ EPR signal observed in inhibited PSII samples at room temperature, we will refer to the low-temperature signal as the broad $S_2Y_Z^•$ EPR signal and the room-temperature signal as the narrow $Y_Z^•$ EPR signal.

The $S_2Y_Z^•$ EPR signal in acetate-inhibited PSII is the first in which both paramagnets display characteristic spectral signatures, corroborating the fact that the S_2-state multiline form of the Mn_4 cluster and $Y_Z^•$ are the paramagnets involved in the interaction. Analysis of the spin−spin interactions between the Mn_4 cluster and $Y_Z^•$ in the $S_2Y_Z^•$ intermediate provides important structural information for development of a model of the Mn_4-Y_Z site which takes into account the proposed importance of Y_Z in water oxidation chemistry (*21*, *28*−*31*). The aim of this work is to characterize the mutual structural and magnetic interactions between Y_Z and the Mn_4 cluster in the $S_2Y_Z^•$ state. We find that the $S_2Y_Z^•$ EPR signal in acetate-inhibited samples is in the static limit below 20 K. Above 30 K, the ^{55}Mn hyperfine features associated with the S_2-state multiline EPR signal become undetectable and the broadened spectrum associated with $Y_Z^•$ begins to narrow dramatically. We interpret the line width narrowing of the $S_2Y_Z^•$ EPR spectrum in acetate-inhibited PSII samples to be due to averaging of the spin−spin interactions between $Y_Z^•$ and the S_2 state caused by an increase in the spin−lattice relaxation rate of the Mn_4 cluster. The temperature dependence exhibited by the $S_2Y_Z^•$ EPR signal in acetate-inhibited PSII is consistent with the known temperature-dependent properties of the S_2-state multiline form of the Mn_4 cluster (*32*). Comparison of temperature-dependent spectra of the $S_2Y_Z^•$ EPR signal in acetate-inhibited, calcium-depleted, and fluoride-substituted PSII leads us to conclude that differences in the $S_2Y_Z^•$ EPR signal line widths for various inhibited samples could be due to variations in the spin state and/or spin−lattice relaxation rate of the Mn_4 cluster created by each of the inhibitory treatments rather than due to major structural differences.

The temperature dependence studies of the $S_2Y_Z^•$ EPR signal presented here demonstrate that the S_2 state in its multiline form is coupled to $Y_Z^•$ in the $S_2Y_Z^•$ intermediate in acetate-inhibited PSII at all temperatures. Previous results, however, show that when acetate-inhibited samples are limited to one turnover with DCMU, only the $g = 4.1$ form of the S_2 state is generated (*23*). These observations raise the possibility that oxidation of Y_Z induces the Mn_4 cluster to convert from the $g = 4.1$ form (spin $\geq {}^3/_2$) to the multiline form (spin $= {}^1/_2$) of the S_2 state. By examining 200 K decay kinetics of the $S_2Y_Z^•$ EPR signal in acetate-treated PSII, we find that no noninteracting S_2-state multiline EPR signal is formed as an intermediate in the decay. This result indicates that the multiline form of the S_2 state is present only when Y_Z is oxidized in acetate-inhibited PSII and suggests that a change in the redox state of Y_Z is coupled to the observed spin-state change of the Mn_4 cluster, possibly through changes in hydrogen bonding associated with Y_Z. Combining the results presented in this work with earlier results (*20*, *23*), we consider the importance of the oxidation state of Y_Z on the properties of the Mn_4 cluster and the local Mn_4-Y_Z environment.

EXPERIMENTAL PROCEDURES

Chemicals and Reagents. MES was purchased from Sigma. Ethylene glycol, DMSO, and sucrose were purchased from Baker. Anhydrous sodium acetate and potassium fluoride were purchased from Fisher Chemical. Sodium chloride was purchased from Mallinckrodt. PPBQ was purchased from Aldrich. All reagents were used without further purification. PPBQ stock solutions (25 mM) were prepared in DMSO and frozen until use.

PSII Sample Preparations. PSII membranes were isolated from market spinach leaves following the procedure of Berthold et al. (*33*) with the modifications of Beck et al. (*34*) except that thylakoid membranes were not stored at 77 K before isolation of PSII membranes. PSII membranes were stored at 77 K in 15 mM NaCl, 20 mM MES, and 30% (v/v) ethylene glycol at pH 6.0, at chl concentrations of approximately 6−8 mg of chl mL^{-1} until use. Chlorophyll concentrations were measured according to the method of Arnon (*35*) on a Perkin-Elmer Lambda 3b UV−vis spectrophotometer. O_2 evolution rates varied from 350 to 450 μmol of O_2 (mg of chl)$^{-1}$ h^{-1} for untreated PSII membranes, as measured by a Clark electrode using the method of Beck et al. (*34*). Acetate-treated PSII membranes were prepared as described by Szalai and Brudvig (*20*). Samples treated with nitric oxide were prepared as described by Szalai and Brudvig (*23*). Manganese-depleted PSII membranes were prepared by 5 mM hydroxylamine treatment as described by Tamura and Cheniae (*36*) and resuspended in 5 mM MES (pH 6.5). Calcium-depleted PSII membranes in buffer containing 0.4 M sucrose, 25 mM MES (pH 6.5), 100 mM NaCl, and 100 μM EGTA were prepared as described by Kalosaka et al. (*25*). Fluoride-substituted PSII membranes were prepared by two washes with a buffer containing 0.3 M sucrose, 40 mM MES (pH 5.5), and 200 mM potassium fluoride. PPBQ was added to acetate-treated, Mn-depleted, calcium-depleted, and fluoride-substituted samples to a final concentration of 500 μM.

EPR Spectroscopy. X-Band EPR spectroscopic measurements at temperatures between 100 and 293 K were performed on a Bruker ER 200 EPR spectrometer equipped with a TM_{110} mode cavity and interfaced to a Macintosh IIci computer. A Bruker nitrogen-flow cryostat assembly was used to maintain temperatures between 100 and 250 K. A Varian E-9 EPR spectrometer equipped with a TE_{102} mode cavity and an Oxford Instruments ESR 900 liquid helium cryostat and interfaced to a Macintosh IIci computer was used for EPR measurements between 4.9 and 80 K. EPR spectra at 2.0 K were collected on a home-built EPR spectrometer (*37*) equipped with an Oxford Instruments ESR 910 liquid helium cryostat and interfaced to a Macintosh IIx computer. For EPR data acquisition at room temperature, samples were centrifuged into a custom-made Wilmad TE quartz flat cell with a fused bottom. For EPR data acquisition at 250 K, a homemade Plexiglas flat cell was used. For EPR

data acquisition at cryogenic temperatures, standard quartz EPR sample tubes were used.

For measurements of the narrow $Y_Z^\bullet$ and $Y_D^\bullet$ and broad $S_2Y_Z^\bullet$ EPR signals at cryogenic temperatures, acetate-treated, calcium-depleted, and fluoride-substituted PSII membranes were illuminated for 5 s at 293 K and cooled to 77 K. For measurements of the $Y_Z^\bullet$ EPR signal at room temperature, acetate-treated and Mn-depleted PSII membranes were continuously illuminated during data acquisition. For measurements of the $Y_D^\bullet$ EPR signal both at room temperature and at low temperatures, samples were dark-adapted for 5 min at 293 K following illumination before recording the spectrum or freezing the sample.

Decay kinetics of the narrow $Y_Z^\bullet$ EPR signal in acetate-treated PSII were determined at 293 and 250 K. At 293 K, samples were illuminated inside the cavity for 15−30 s. The postillumination signal intensity was measured as the transient decay of the low-field hyperfine peak of the $Y_Z^\bullet$ signal. For the 250 K measurements, the sample was illuminated for 5 s at 293 K and immediately transferred to the EPR cryostat which was maintained at 250 K, and the full $Y_Z^\bullet$ EPR spectrum was collected as a function of 250 K dark incubation time in the cavity. The corresponding decay of the $S_2Y_Z^\bullet$ EPR signal intensity was monitored at 6 K as a function of dark incubation time at 293 or 250 K (CCl_4/dry ice slurry) (*20*). The decay of the $S_2Y_Z^\bullet$ EPR signal intensity and formation of the S_2-state $g = 4.1$ EPR signal were measured at 10 K after dark incubation at 200 K (acetone/dry ice slurry).

The microwave powers at half-saturation ($P_{1/2}$) were calculated from least-squares fits of eq 1 with b fixed at the inhomogeneous limit of 1

$$\text{intensity} = \frac{K\sqrt{P}}{(1 + P/P_{1/2})^{b/2}} \qquad (1)$$

where P is the microwave power, K is a scaling constant, and b is the inhomogeneity factor (*38*).

For power−saturation studies, the signal intensities of the narrow $Y_D^\bullet$ and $Y_Z^\bullet$ EPR signals were determined by double integration; the intensity of the broad $S_2Y_Z^\bullet$ EPR signal was measured as the peak-to-trough amplitude, and the S_2-state multiline EPR signal intensity was estimated as the sum of four to six low-field hyperfine peak amplitudes. The S_2-state $g = 4.1$ EPR signal was measured as the peak-to-trough height in light-minus-dark difference spectra.

Integrated areas were measured to test for Curie law behavior. For both the broad $S_2Y_Z^\bullet$ EPR signal (below 80 K) and the narrow $Y_Z^\bullet$ EPR signal (above 100 K), the area was measured after subtraction of the EPR signal from $Y_D^\bullet$, as described by Szalai and Brudvig (*20*). The widths of the $S_2Y_Z^\bullet$ EPR signal were measured both as the peak-to-trough separation in the first-derivative spectra and the full width at half-height of the absorption signals obtained by integrating the first-derivative spectra; both measurements gave similar values.

RESULTS AND DISCUSSION

When acetate-inhibited PSII samples are illuminated for short times at room temperature and then cooled to cryogenic temperatures, the broad EPR signal assigned to $Y_Z^\bullet$ interacting with the S_2 state is observed (Figure 1A). The EPR spectrum in Figure 1A shows the main "split-signal" feature of the $S_2Y_Z^\bullet$ EPR signal, which is also found for other inhibited samples, and the ^{55}Mn hyperfine peaks on the low- and high-field portions of the signal which have only been observed in the $S_2Y_Z^\bullet$ EPR signal of acetate-inhibited PSII (*19*, *20*, *39*). The ^{55}Mn hyperfine peaks which appear with the main $S_2Y_Z^\bullet$ EPR signal peaks do not arise from uninhibited PSII centers in the S_2 state because 200 K illumination of acetate-treated centers does not produce the S_2-state multiline EPR signal. Additionally, acetate-inhibited centers limited to one turnover and illuminated at temperatures above 250 K display only the $g = 4.1$ form of the S_2

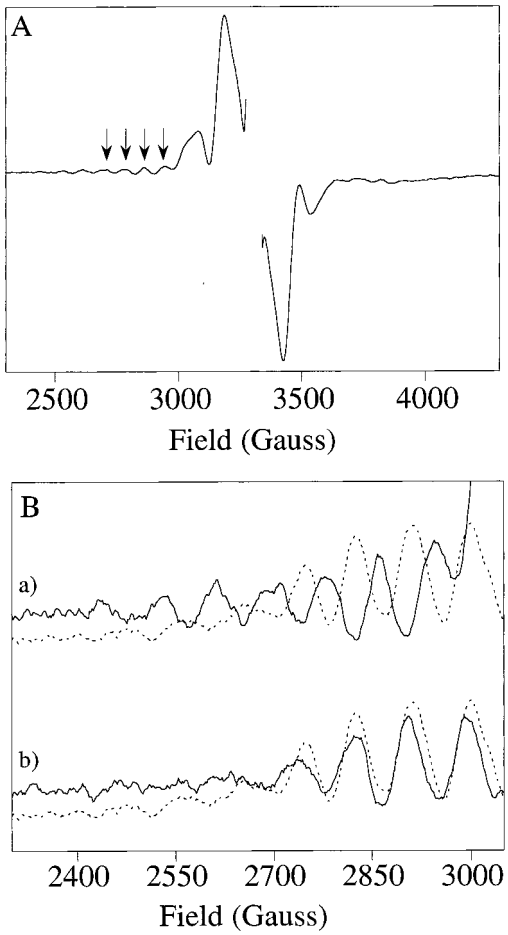

FIGURE 1: Comparison of the $S_2Y_Z^\bullet$ EPR signal in acetate-treated PSII, the S_2-state multiline EPR signal in untreated PSII, and the S_2-state multiline EPR signal in acetate- and NO-treated PSII. (A) $S_2Y_Z^\bullet$ EPR signal in acetate-treated PSII. The central region corresponding to the EPR signal from $Y_D^\bullet$ has been removed for clarity. The arrows indicate ^{55}Mn hyperfine peaks associated with the $S_2Y_Z^\bullet$ EPR signal that were used for quantitation (see the text). (B) Low-field region of spectra showing ^{55}Mn hyperfine peaks: (a) solid line, ^{55}Mn hyperfine peaks associated with the $S_2Y_Z^\bullet$ EPR signal in acetate-treated PSII; and dashed line, ^{55}Mn hyperfine peaks of the S_2-state multiline EPR signal in untreated PSII; and (b) solid line, ^{55}Mn hyperfine peaks associated with acetate- and NO-treated PSII in the S_2Y_Z−NO state [sample prepared as described by Szalai and Brudvig (*23*)]; and dashed line, same as dashed line in part a. The spectra have been scaled to have comparable amplitudes of the ^{55}Mn hyperfine peaks. EPR instrumental parameters were as follows: microwave frequency, 9.28 GHz; magnetic field modulation frequency, 100 kHz; magnetic field modulation amplitude, 20 G; microwave power, 20 mW; and temperature, 8 K, except for the data for the solid line in part b in which the microwave power was 5 mW and the temperature was 6 K.

state (*23*). Figure 1B shows the low-field hyperfine features associated with the $S_2Y_Z^\bullet$ EPR signal on an expanded scale in comparison to the S_2-state multiline EPR signal from an untreated sample and the S_2Y_Z-NO species formed when the $S_2Y_Z^\bullet$ intermediate is generated in an acetate-inhibited sample in the presence of $NO^\bullet$. Previous work has shown that $NO^\bullet$ binds to $Y_Z^\bullet$ to form a diamagnetic Y_Z-NO species which uncouples the S_2 state from $Y_Z^\bullet$, yielding a noninteracting S_2-state multiline EPR signal species (*23*). The multiline EPR signal observed from the $S_2Y_Z^\bullet$ species is significantly different from that in an untreated sample (Figure 1B, part a). The hyperfine peaks from the $S_2Y_Z^\bullet$ species are offset by about 40 G, although the splittings are not significantly different. We interpret this offset to be due to the spin−spin interaction between $Y_Z^\bullet$ and the S_2 state of the Mn_4 cluster. This interpretation is supported by the observation that the S_2-state multiline EPR signals from an untreated sample and from the S_2Y_Z-NO species are very similar (Figure 1B, part b), even though the latter signal is formed in the presence of acetate. The intensity of the S_2-state multiline EPR signal produced in acetate- and $NO^\bullet$-treated PSII is about 45% of the intensity of the S_2-state multiline EPR signal in an untreated sample; this is the same as the yield of the $S_2Y_Z^\bullet$ EPR signal under equivalent conditions but without nitric oxide (*23*). We have not attempted quantitation of the S_2-state multiline EPR signal features in the $S_2Y_Z^\bullet$ EPR spectrum because the change in the line shape precludes a quantitative comparison with the S_2-state multiline EPR signal in an untreated sample. However, we have measured the intensity ratio of the sum of four of the ^{55}Mn hyperfine peaks (indicated by arrows in Figure 1A) to the peak-to-trough height of the main split signal feature in 10 samples prepared in the $S_2Y_Z^\bullet$ state and found it to be highly reproducible (15.8 ± 4.9%). This would not be the case if the ^{55}Mn hyperfine peaks were from a variable proportion of centers in the S_2 state.

On the basis of these results, we conclude that the spin−spin interaction between the spin $^1/_2$ S_2 state and Y_Z radical gives rise to reciprocal splittings of both EPR signals (*40*, *41*) so that the $S_2Y_Z^\bullet$ interaction spectrum consists of distinguishable contributions from $Y_Z^\bullet$ and the S_2 state. The exchange and dipolar interactions between the Mn_4 cluster and $Y_Z^\bullet$ must be in the weak-coupling regime because reproducible changes at low magnetic field corresponding to a half-field transition were not observed using perpendicular or parallel mode EPR spectroscopies. Splitting of the $Y_Z^\bullet$ EPR signal gives rise to a pair of more intense peaks flanked by a pair of less intense peaks, readily observed on either side of $g = 2$, which is analogous to an AB pattern in NMR spectra (*40*). The EPR signal from the S_2 state has a much smaller intensity and extends over several thousand gauss. Only for the $S_2Y_Z^\bullet$ species in acetate-inhibited PSII does the S_2-state multiline EPR signal exhibit resolved ^{55}-Mn hyperfine structure. This is a consequence of the ^{55}Mn hyperfine coupling constant (80−85 G) being an integral multiple of the spin−spin splitting of 240 G. In the interaction spectrum, the ^{55}Mn hyperfine peaks shift by half of the overall spin−spin splitting, approximately 120 G (*41*). As a result, even though the ^{55}Mn hyperfine peak splitting remains at 80−85 G in the $S_2Y_Z^\bullet$ EPR spectrum, the ^{55}Mn hyperfine peak positions appear to shift by 40 G relative to those in a noninteracting S_2-state multiline EPR spectrum (Figure 1B). More importantly, in acetate-treated PSII, the 120 G shift created by the spin−spin coupling does not cause the ^{55}Mn hyperfine peaks to interfere destructively so that they disappear into the baseline. This may not be the case for other inhibited PSII samples which exhibit $S_2Y_Z^\bullet$ EPR signals lacking a resolved S_2-state multiline EPR signal. In calcium-depleted PSII, the contribution from the S_2 state to the $S_2Y_Z^\bullet$ EPR signal has been modeled as an underlying broad unresolved 2000 G-wide signal (*42*, *43*). Alternatively, inhibited samples other than acetate-inhibited samples may lack observable S_2-state EPR signals because of effects of the inhibitory treatments on the magnetic properties of the S_2 state and temperature-dependent line broadening (see below).

Table 1: $P_{1/2}$ Values Calculated from Microwave Power Saturation Data

signal	sample	T (K)	$P_{1/2}$ (mW)
$S_2Y_Z^\bullet$ ($Y_Z^\bullet$ peak)	acetate-inhibited	5.0	0.36
		5.4	0.62
		5.7	1.2
		6.0	1.7
		7.5	18
		20	>100
$S_2Y_Z^\bullet$ (^{55}Mn hyperfine peaks)	acetate-inhibited	6.0	6.7
$Y_Z^\bullet$	acetate-inhibited	293	>100
$Y_Z^\bullet$	Mn-depleted	293	12
$S_1Y_D^\bullet$	acetate-inhibited	20	1.6
		293	11
$Y_D^\bullet$	Mn-depleted	293	16

Microwave Power Saturation. One way to address the nature of the interaction between $Y_Z^\bullet$ and the Mn_4 cluster is to measure the saturation behavior of the $Y_Z^\bullet$ EPR signal as a function of temperature. If $Y_Z^\bullet$ is coupled to the S_2 state at all temperatures, then the $P_{1/2}$ of $Y_Z^\bullet$ should be much higher than the $P_{1/2}$ of $Y_D^\bullet$ or $Y_Z^\bullet$ in a Mn-depleted sample. Unfortunately, the EPR signals of $Y_Z^\bullet$ and $Y_D^\bullet$ overlap; they are principally differentiated by decay kinetics and slightly different hyperfine splittings. To deconvolute the two EPR signals, spectra collected after dark incubation, which contain only a $Y_D^\bullet$ contribution, are subtracted from spectra collected during illumination (or after freezing under illumination) which contain both $Y_D^\bullet$ and $Y_Z^\bullet$ components. The resultant light-minus-dark difference spectrum contains only the EPR signal from $Y_Z^\bullet$ if nonsaturating microwave powers are used.

Panels A and B of Figure 2 show microwave power saturation data for acetate-inhibited PSII (solid symbols) in comparison to data for Mn-depleted PSII (open symbols). $P_{1/2}$ values are listed in Table 1. In acetate-inhibited PSII, the $S_2Y_Z^\bullet$ EPR signal observed at low temperatures and the narrow $Y_Z^\bullet$ EPR signal observed at room temperature do not reach saturation up to microwave powers of 100 mW, indicating that the spin relaxation of $Y_Z^\bullet$ is strongly enhanced by the Mn_4 cluster both at low and high temperatures. Similar room-temperature power−saturation behavior for $Y_Z^\bullet$ was observed by Yocum and Babcock in ammonia-treated PSII (*24*). On the other hand, in Mn-depleted PSII, $Y_Z^\bullet$ and $Y_D^\bullet$ are readily saturated and they have equivalent power−saturation behavior, consistent with past work (*44*).

Figure 2C shows a comparison between the power−saturation behavior of the main "split signal" feature of the $S_2Y_Z^\bullet$ EPR signal and one of the ^{55}Mn hyperfine peaks. The split signal feature is more easily saturated. The reason that

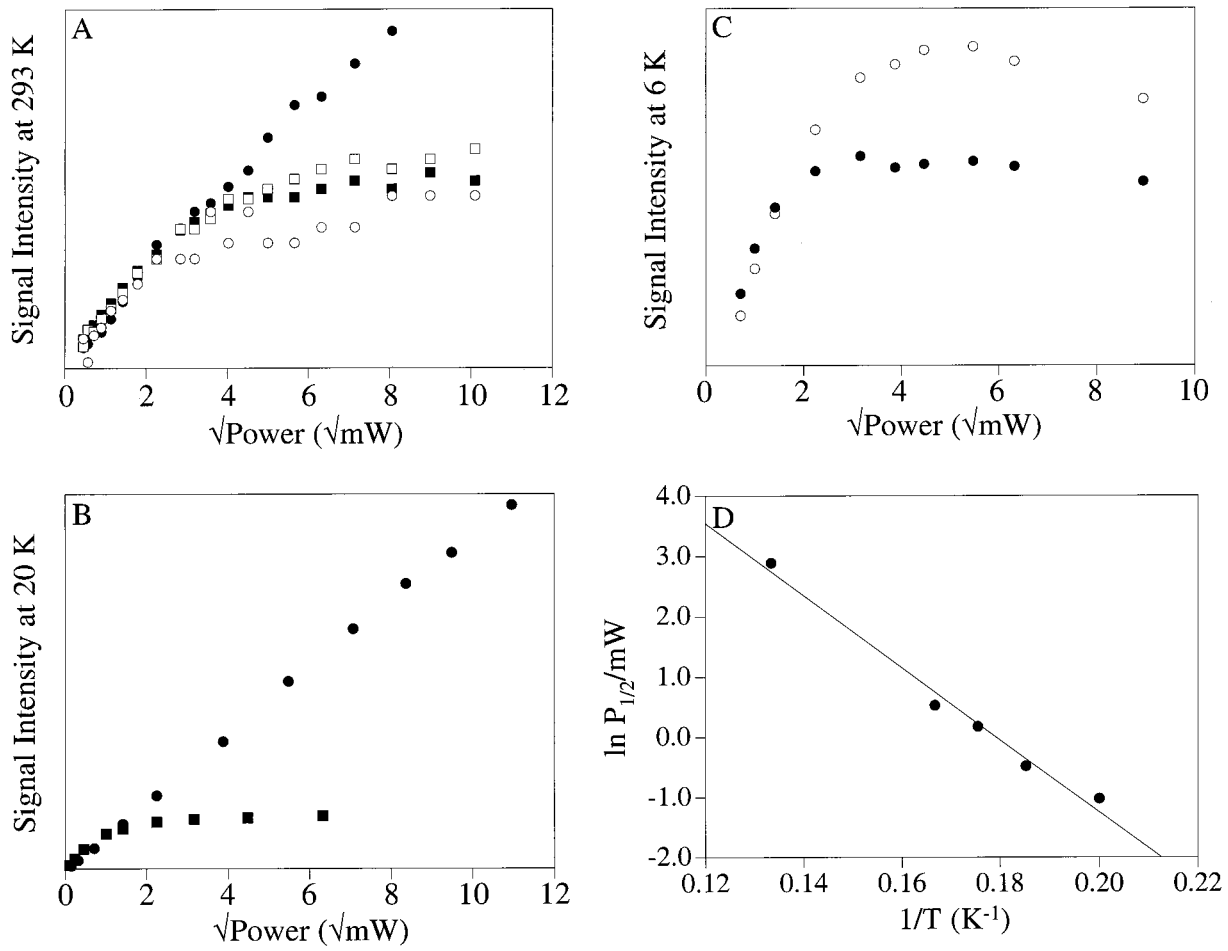

FIGURE 2: Microwave power saturation of the EPR signals from $Y_Z^\bullet$, $Y_D^\bullet$, $S_2Y_Z^\bullet$, and ^{55}Mn hyperfine peaks associated with the $S_2Y_Z^\bullet$ EPR signal in acetate-treated, untreated, and Mn-depleted PSII. (A) $Y_Z^\bullet$ and $Y_D^\bullet$ EPR signals recorded at 293 K: (●) narrow $Y_Z^\bullet$ EPR signal intensity in acetate-treated PSII ($S_2Y_Z^\bullet$), (■) dark-stable $Y_D^\bullet$ EPR signal intensity in acetate-treated PSII ($S_1Y_D^\bullet$), (○) narrow $Y_Z^\bullet$ EPR signal intensity in Mn-depleted PSII, and (□) dark-stable $Y_D^\bullet$ EPR signal intensity in Mn-depleted PSII. (B) $S_2Y_Z^\bullet$ and $Y_D^\bullet$ EPR signals recorded at 20 K: (●) light-induced $S_2Y_Z^\bullet$ EPR signal intensity in acetate-treated PSII and (■) $Y_D^\bullet$ EPR signal intensity in acetate-treated PSII ($S_1Y_D^\bullet$). (C) $S_2Y_Z^\bullet$ EPR signal recorded at 6 K. Data are the average of two experiments: (●) light-induced $S_2Y_Z^\bullet$ EPR signal intensity in acetate-treated PSII and (○) intensity of one of the ^{55}Mn hyperfine peaks associated with the $S_2Y_Z^\bullet$ EPR signal in acetate-treated PSII. (D) Orbach plot of $P_{1/2}$ of the $S_2Y_Z^\bullet$ EPR signal. The $P_{1/2}$ data used for the plot are compiled in Table 1. The solid line is a linear fit to the data. EPR instrumental parameters were as follows: microwave frequency, (A) 9.68 and (B−D) 9.28 GHz; magnetic field modulation frequency, 100 kHz; and magnetic field modulation amplitude, (A) 4 G, (B) 20 G for $S_2Y_Z^\bullet$ and 4 G for $Y_D^\bullet$, and (C and D) 20 G. Intensities were measured as described in the text. For panels A−C, data sets were normalized to an initial slope of 1.

both features do not reach saturation at the same powers, even though they arise from the $S_2Y_Z^\bullet$ state, may be because the strong-coupling limit has not been reached. Nonetheless, the temperature dependence of the spin relaxation of $Y_Z^\bullet$ should reflect its relaxation enhancement by the S_2 state. Figure 2D shows an Orbach plot of the $P_{1/2}$ values of the split signal feature of the $S_2Y_Z^\bullet$ EPR signal. For an Orbach relaxation mechanism, $P_{1/2}$ values are proportional to $\exp(-\Delta/kT)$, where Δ is the energy separation between the ground and first excited spin-state manifolds (*45*). A plot of ln $P_{1/2}$ versus $1/T$ should be linear with a slope of $-\Delta/k$. Figure 2D shows a linear fit giving a Δ of 42 ± 5 cm^{-1}. This value is comparable to those obtained by the same method assuming an Orbach relaxation process for the S_2-state multiline EPR signal in untreated samples (*32*, *46*−*48*).

EPR Signal Decay Kinetics. In acetate-treated PSII, both the narrow $Y_Z^\bullet$ EPR signal observed at higher temperatures and the broad $S_2Y_Z^\bullet$ EPR signal observed at low temperatures are induced by room-temperature illumination. After the initial room-temperature illumination, the loss of EPR signal intensity due to decay reactions can be measured as a function of dark incubation time. Matching decay kinetics at several temperatures would indicate that the $Y_Z^\bullet$ and $S_2Y_Z^\bullet$ EPR signals arise from the same population of $Y_Z^\bullet$. As shown in Figure 3, the decays of both the narrow $Y_Z^\bullet$ EPR signal and the broad $S_2Y_Z^\bullet$ EPR signal exhibit the same kinetics. When fit with a single-exponential decay equation, the rate constant of the decay at room temperature (293 K) is 1.6 ± 0.2 min^{-1}. This value is somewhat higher than the decay constant of 0.87 ± 0.06 min^{-1} at 294 K published earlier (*20*), because the previous study did not take into account the delay introduced by the freezing process. We conclude that the same $S_2Y_Z^\bullet$ species gives rise to both the narrow and broad $Y_Z^\bullet$ EPR signals observed at room and cryogenic temperatures, respectively.

Temperature Dependence of EPR Signal Line Shapes. At cryogenic temperatures, acetate-treated PSII displays a broad $S_2Y_Z^\bullet$ EPR signal, which narrows as the temperature is increased (Figure 4A). As the signal narrows, the total signal intensity multiplied by temperature remains constant, following Curie law behavior (data not shown). Below 20 K,

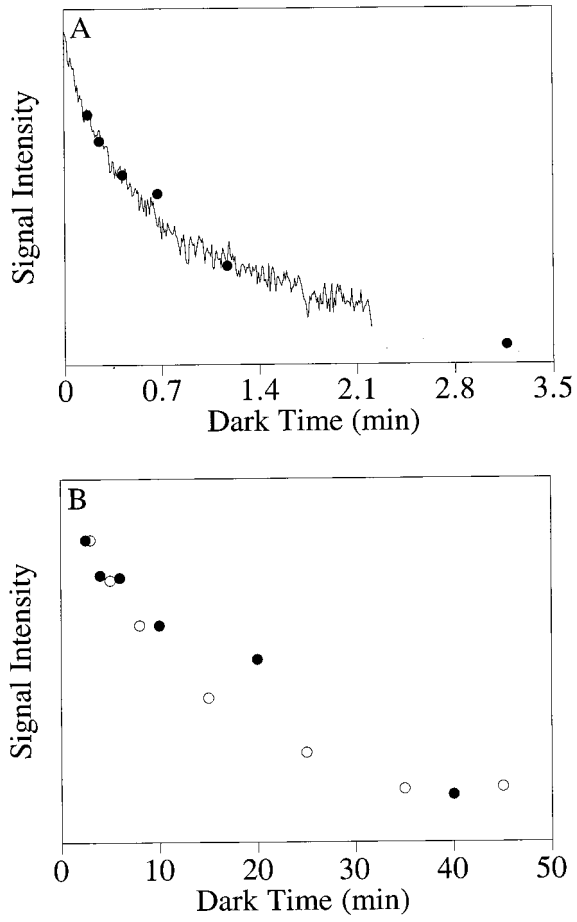

FIGURE 3: Decay kinetics of the EPR signals from $Y_Z^\bullet$ in acetate-treated PSII. (A) Decays at 293 K: (●) $S_2Y_Z^\bullet$ EPR signal peak height recorded at 6 K and (solid line) narrow $Y_Z^\bullet$ signal peak height recorded at 293 K. The initial point of the data set collected at 6 K was offset from time zero by 10 s, to account for freezing time, and it was normalized to the height of the 293 K data set at 10 s. (B) Decays at 250 K: (●) $S_2Y_Z^\bullet$ EPR signal peak height recorded at 6 K and (○) narrow $Y_Z^\bullet$ EPR signal peak height recorded at 250 K. EPR instrumental parameters were as follows: microwave frequency, 9.68 GHz at 293 K, 9.46 GHz at 250 K, and 9.28 GHz at 6 K; magnetic field modulation frequency, 100 kHz; magnetic field modulation amplitude, 4 G at 293 and 250 K and 20 G at 6 K; microwave power, 2.0 mW at 293 and 250 K and 5.0 mW at 6 K; and instrumental time constant for 293 K measurements, 200 ms.

acetate-treated PSII membranes exhibit the characteristic ~240 G-wide $S_2Y_Z^\bullet$ EPR signal. As the temperature is raised to 40 K, the signal narrows to ~150 G. No narrow component of the light-induced signal corresponding to $Y_Z^\bullet$ is observed at these temperatures (Figure 4B; see also refs *20* and *49*). When the temperature is increased further, the $S_2Y_Z^\bullet$ EPR signal continues to narrow and becomes undetectable at approximately 80 K. Near this temperature, a narrow EPR signal from $Y_Z^\bullet$ begins to grow in, as evidenced by the intensity on the wings of the $Y_D^\bullet$ EPR signal in Figure 4B (parts c and d). At 116 K, a narrow $Y_Z^\bullet$ EPR signal is observed that is similar to that observed at room temperature (*26*), although its line width is broader. The $Y_Z^\bullet$ EPR signal continues to narrow as the temperature is increased, resulting in better resolution of the hyperfine structure. Over the entire temperature range, the $S_2Y_Z^\bullet$ state exhibiting either the broad $S_2Y_Z^\bullet$ EPR signal or the narrow $Y_Z^\bullet$ EPR signal does not reach saturation at microwave powers of up to 100 mW, as shown in Table 1 at the low- (20 K) and high-temperature

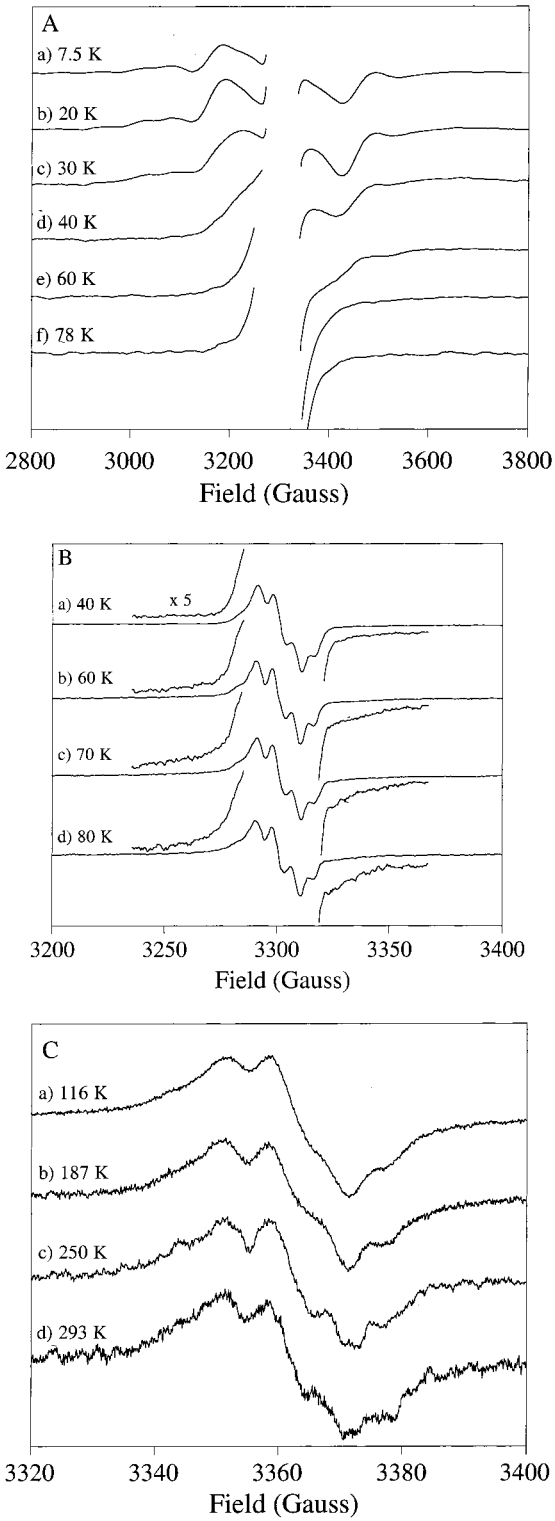

FIGURE 4: Temperature dependence of $S_2Y_Z^\bullet$ EPR signal line shapes in acetate-treated PSII from 7.5 to 293 K. (A) Wide scans (light-minus-dark difference spectra) at low temperatures. Full signal widths at half-height: (a) 240, (b) 235, (c) 190, (d) 100, (e) 77, and (f) 64 G. The sharp central feature from $Y_D^\bullet$ has been removed. (B) Narrow scans (light spectra) at low temperatures. (C) Narrow scans (light-minus-dark difference spectra) at high temperatures. EPR instrumental parameters were as follows: microwave frequency, (A and B) 9.28 GHz and (C) (a−c) 9.45 and (d) 9.68 GHz; magnetic field modulation frequency, 100 kHz; magnetic field modulation amplitude, (A) 20, (B) 4, (C) (a−c) 4, and (d) 2 G; and microwave power, (A) 40, (B) 0.5, (C) (a−c) 0.02, and (d) 2 mW. Spectra in panels A and B are scaled assuming Curie law behavior.

(293 K) limits. This is the first time that the EPR signal from $Y_Z^\bullet$ in treated PSII samples has been mapped at intermediate temperatures. These data indicate that progressive narrowing of the $S_2Y_Z^\bullet$ EPR signal occurs such that above 80 K its line shape resembles that of a noninteracting tyrosyl radical.

By using the known values of T_1 for the S_2-state multiline EPR signal species in untreated samples, we can estimate the temperature at which averaging of the interaction between the S_2 state and $Y_Z^\bullet$ should occur. The peak-to-trough separation of the main split signal feature of the $S_2Y_Z^\bullet$ EPR signal is 240 G which corresponds to an interaction of about 0.03 cm^{-1}. Spectral simulation of the $S_2Y_Z^\bullet$ EPR signal in acetate-inhibited PSII gives an exchange coupling constant of -0.028 cm^{-1} (*41*, *50*). Using 0.03 cm^{-1} for the interaction and the equation $T_1 = 2\sqrt{2}/\Delta\omega$ (*51*), where $\Delta\omega$ is the peak-to-trough splitting in s^{-1} rad^{-1}, the calculated value of T_1 at which averaging of the S_2 state$-Y_Z^\bullet$ interaction should begin to occur is 8.9×10^{-11} s. In comparison, T_1 for the S_2-state multiline EPR signal species in untreated PSII is 5.6×10^{-7} s at 11 K, and $1/T_1$ has a T^6 temperature dependence (*32*). Extrapolating to higher temperatures gives 33 K for the temperature at which T_1 would be 8.9×10^{-11} s and the S_2 state$-Y_Z^\bullet$ interaction should begin to be averaged. Our results show that the $S_2Y_Z^\bullet$ EPR signal begins to narrow noticeably at about 30 K (Figure 4A). This calculation assumes that the T^6 temperature dependence of the S_2-state spin$-$lattice relaxation rate measured by Lorigan and Britt (*32*) in untreated PSII also holds for acetate-inhibited PSII samples. Our observation that the $P_{1/2}$ values of the $S_2Y_Z^\bullet$ EPR signal display a temperature dependence similar to that of the S_2-state multiline EPR signal species in untreated PSII (Figure 2D) gives support for this assumption. These results are consistent with relaxation enhancement of $Y_Z^\bullet$ by the S_2-state multiline EPR signal species at both room and cryogenic temperatures.

On the basis of these results, the decay kinetics, and the enhanced relaxation properties of both EPR signals, we conclude that the broad $S_2Y_Z^\bullet$ EPR signal observed at low temperatures and the narrow $Y_Z^\bullet$ EPR signal observed at room temperature are manifestations of the same interaction. The temperature-dependent line shape changes of the $S_2Y_Z^\bullet$ EPR signal are consistent with an increase in the spin$-$lattice relaxation rate of the Mn_4 cluster as the temperature is raised (see above). Because of fast spin$-$lattice relaxation of the Mn_4 cluster, the spin$-$spin coupling between $Y_Z^\bullet$ and the Mn_4 cluster is averaged as the temperature increases. Such averaging of spin$-$spin interactions by fast spin relaxation has been observed for other exchange- and dipolar-coupled systems in which one of the spins is a transition metal and the other is a nitroxide radical (*52*, *53*).

Different inhibitory treatments of PSII produce $S_2Y_Z^\bullet$ EPR signals with varying widths (*13*, *17*, *19*). The narrowing of the $S_2Y_Z^\bullet$ EPR signal in acetate-treated PSII with temperature suggests that the $S_2Y_Z^\bullet$ EPR signal line shapes produced by different treatments may be due to variations in the magnetic properties of the Mn_4 cluster. One way to address this question is to examine the temperature dependence of the $S_2Y_Z^\bullet$ EPR signals from fluoride-treated and calcium-depleted PSII samples. The line width of the $S_2Y_Z^\bullet$ EPR signal in acetate-treated PSII at 40 K is similar to that of the $S_2Y_Z^\bullet$ EPR signals in calcium-depleted and fluoride-substituted samples at 10 K (Figures 4A and 5). Below 20 K, the width of the $S_2Y_Z^\bullet$ EPR signal in acetate-treated samples does not broaden further (Figure 4A). Spectra of a calcium-depleted sample at 10 and 2 K look approximately the same, although the measured line width is somewhat broader at 2 K. As the temperature is raised to 40 K, the $S_2Y_Z^\bullet$ EPR signal in the calcium-depleted PSII sample narrows to 108 G. In a fluoride-substituted sample, on the other hand, the signal shows significant broadening on cooling from 10 to 2 K, where it is ~200 G wide (Figure 5). When the temperature is increased to 25 K, the $S_2Y_Z^\bullet$ EPR signal in fluoride-substituted PSII narrows to 116 G, which is approximately the same width as that found for acetate-inhibited and calcium-depleted samples at 60 and 40 K, respectively. This means that calcium-depleted and acetate-treated PSII samples reach a static limit at higher temperatures than fluoride-substituted samples. The finding that the $S_2Y_Z^\bullet$ EPR signal of fluoride-substituted PSII continues to broaden at temperatures lower than those of acetate-treated PSII samples supports the idea that different inhibitory treatments affect the magnetic properties of the Mn_4 cluster. Fluoride induces the $g = 4.1$ form of the S_2 state (*17*, *54*$-$*56*). Therefore,

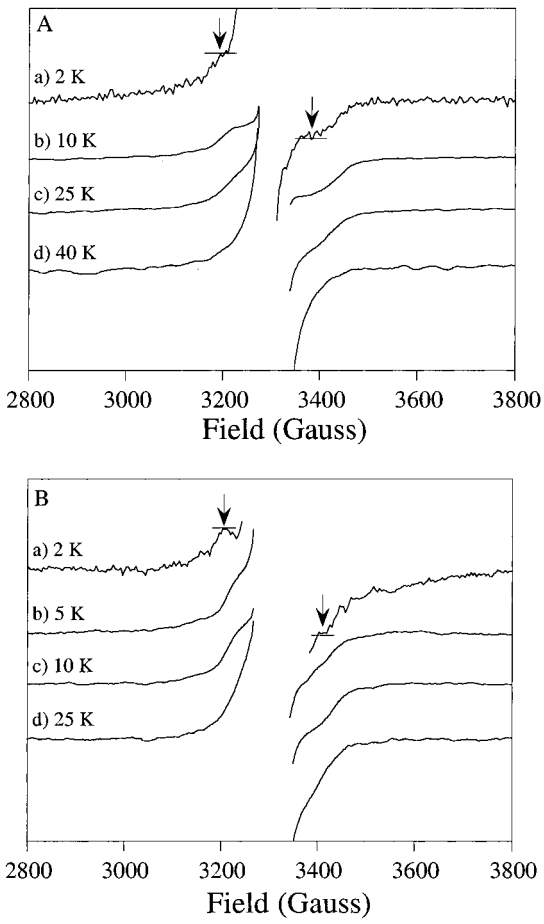

FIGURE 5: EPR line shapes of $S_2Y_Z^\bullet$ EPR signals in (A) calcium-depleted and (B) fluoride-substituted PSII. The EPR spectrum of the $S_2Y_Z^\bullet$ EPR signal in acetate-treated PSII was also measured at 2 K (data not shown) and matches that at 7.5 K (Figure 4A, spectrum a). EPR instrumental parameters were as follows: (A and B), microwave frequency, 9.28 GHz except for (a) 9.07 GHz; magnetic field modulation frequency, 100 kHz; magnetic field modulation amplitude, 20 G; (A) microwave power, (a) 0.02, (b) 10, (c) 25, and (d) 50 mW; and (B) microwave power, (a) 0.02, (b) 1, (c) 10, and (d) 25 mW.

the different temperature dependence of the line width of the $S_2Y_Z^\bullet$ signal in fluoride-substituted PSII may be a result of a different spin state of the Mn_4 cluster. In this context, the line width differences of the $S_2Y_Z^\bullet$ EPR signals in different inhibited samples may be due to variations in the spin state and/or the spin−lattice relaxation rate of the Mn_4 cluster, rather than to significant differences in the Mn_4-Y_Z structure. This interpretation would explain the varying line widths for the $S_2Y_Z^\bullet$ EPR signal in different inhibited samples even though all samples are blocked at the same catalytic step (*13*, *17*−*19*, *57*).

Spin-State Conversion of the Mn_4 Cluster. Acetate-inhibited PSII samples limited to one turnover with DCMU and illuminated at temperatures above 250 K produce only the $g = 4.1$ form of the S_2 state (*23*). Similarly, the S_2 state $g = 4.1$ EPR signal is observed upon decay of the $S_2Y_Z^\bullet$ EPR signal at temperatures above 250 K in acetate-inhibited samples (*20*). Although the $g = 4.1$ form of the S_2 state is implicated in the formation and decay pathway of the $S_2Y_Z^\bullet$ intermediate in acetate-inhibited PSII, experiments using nitric oxide to quench the $S_2Y_Z^\bullet$ EPR signal have shown that the paramagnet coupled to $Y_Z^\bullet$ in the $S_2Y_Z^\bullet$ state is the multiline form of the S_2 state (*23*). To confirm that the multiline form of the S_2 state is present only when it is interacting with $Y_Z^\bullet$, we have measured the decay kinetics of the $S_2Y_Z^\bullet$ intermediate at 200 K in acetate-treated PSII (Figure 6). Previously, we attributed the ^{55}Mn hyperfine features of the $S_2Y_Z^\bullet$ EPR signal to a fractional yield of the S_2-state multiline EPR signal formed upon decay of the $S_2Y_Z^\bullet$ intermediate (*23*). The current data show that the field positions of the ^{55}Mn hyperfine features associated with the $S_2Y_Z^\bullet$ EPR signal remain shifted from those of the non-interacting S_2 state throughout the time course of dark incubation at 200 K (Figure 6A). All of the features associated with the $S_2Y_Z^\bullet$ EPR signal decay on the same time scale, and perhaps not surprisingly, the S_2-state $g = 4.1$ EPR signal is formed on the same time scale in which the $S_2Y_Z^\bullet$ EPR signal decays (Figure 6B). Therefore, we conclude that the S_2-state multiline EPR signal is not an intermediate in the decay.

Exclusive observation of the S_2-state $g = 4.1$ EPR signal upon decay of the $S_2Y_Z^\bullet$ EPR signal suggests that reduction of $Y_Z^\bullet$ triggers a change in the spin state of the Mn_4 cluster from the multiline form (spin = $^1/_2$) to the $g = 4.1$ form (spin ≥ $^3/_2$) in acetate-inhibited PSII. In conjunction with previous results (*20*, *23*), these data support the idea that a close link exists between the Mn_4 cluster and Y_Z in acetate-inhibited PSII, both spatially as determined by analyses of the spin−spin interaction in the $S_2Y_Z^\bullet$ intermediate (*21*, *39*, *41*, *42*, *50*, *58*) and structurally as shown by the effect of Y_Z oxidation and/or $Y_Z^\bullet$ reduction on the spin state of the Mn_4 cluster.

Because $Y_Z^\bullet$ is a neutral tyrosine radical (*59*), the proton associated with reduced Y_Z is donated to a nearby base, probably D1 His190 (*60*−*63*), when $Y_Z^\bullet$ is formed. Therefore, upon oxidation of S_2Y_Z to form the $S_2Y_Z^\bullet$ intermediate, the primary difference expected in the environment of the OEC is a change in hydrogen-bonding interactions of Y_Z. Recent Fourier transform infrared spectroscopy measurements of the S_1 to S_2 transition reveal that a tyrosine residue is structurally coupled to the Mn_4 cluster through either a hydrogen-bonded network or direct hydrogen-bonding interactions (*64*). The spin-state change of the Mn_4 cluster that we observe upon Y_Z oxidation and/or $Y_Z^\bullet$ reduction supports the view that hydrogen-bonding changes near Y_Z are propagated to the Mn_4 cluster through such a hydrogen-bonded network, potentially involving a ligand directly bound to the Mn_4 cluster. Although our conclusions are based on results collected for inhibited PSII samples, this interpretation is consistent with current proposals of the mechanism of water oxidation which include direct participation of $Y_Z^\bullet$ in H-atom abstraction from substrate bound to manganese (*21*, *28*−*31*).

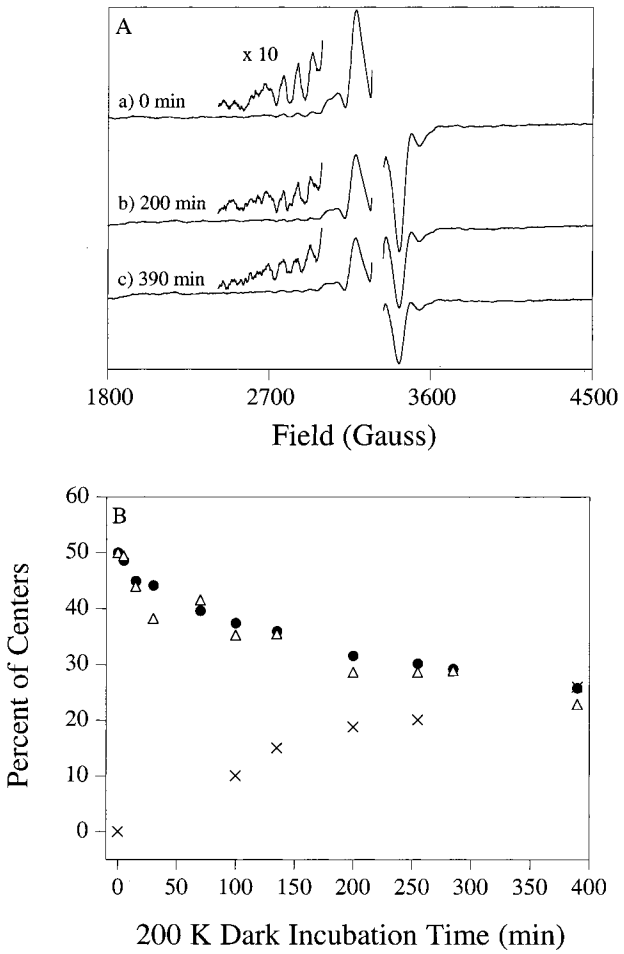

FIGURE 6: (A) Light-minus-dark difference spectra of the $S_2Y_Z^\bullet$ EPR signal as a function of 200 K dark incubation time. (B) Plot of the (●) decay of the main split signal feature of the $S_2Y_Z^\bullet$ EPR signal, (△) decay of the sum of four ^{55}Mn hyperfine peak intensities (see Figure 1A), and (×) formation of the S_2-state $g = 4.1$ EPR signal as a function of dark incubation time at 200 K. The percentage of centers contributing to the $S_2Y_Z^\bullet$ EPR signal was determined as described by Szalai and Brudvig (*20*). The S_2-state $g = 4.1$ EPR signal peak height was normalized to the difference between the initial and final yields of the $S_2Y_Z^\bullet$ EPR signal decay. EPR instrumental parameters were as follows: temperature, 8.0 K; microwave frequency, 9.28 GHz; magnetic field modulation frequency, 100 kHz; magnetic field modulation amplitude, 20 G; and microwave power, 10 mW.

Further evidence for the intimate relationship between Y_Z and the Mn_4 cluster is apparent in the observation that $Y_Z^\bullet$ is not formed by illumination at temperatures below 250 K in Mn-depleted PSII samples, but that Y_Z is transiently oxidized during the S_1 to S_2 transition of the Mn_4 cluster in untreated PSII at temperatures as low as 140 K (*65*). The simplest explanation for this "Y_Z paradox" is that, by

removing or perturbing the Mn_4 cluster, the hydrogen-bonded environment surrounding Y_Z is significantly altered which leads to changes in the redox properties of Y_Z (*28*). In fact, Y_Z oxidization at low temperatures during the S_1 to S_2 transition in untreated PSII suggests that Y_Z must exist in a well-ordered structure so that upon oxidation its proton can be transferred to a nearby base with minimal rearrangement (*66*). When the Mn_4 cluster is removed as in Mn-depleted samples or perturbed as in inhibited PSII preparations, $Y_Z^\bullet$ reduction is slowed and $Y_Z^\bullet$ can be easily observed spectroscopically (*11*, *24*, *25*, *26*, *50*). In part, measurements on Y_Z in Mn-depleted PSII (*11*, *59*) have led to proposals which advocate Y_Z flexibility in the water oxidation process (*21*, *29*, *59*). Unfortunately, precise information about Y_Z oxidation in untreated PSII is not provided by experiments on Y_Z in Mn-depleted PSII since the reactivity of Y_Z is clearly different in the two types of samples. In inhibited PSII samples, $Y_Z^\bullet$ reduction kinetics are not the only facet of Y_Z reactivity which is an indication of a perturbed local Mn_4-Y_Z structure; the S_1 to S_2 transition occurs at illumination temperatures ranging from 200 to 250 K (*17*, *19*, *20*, *67*−*69*), and the $S_2Y_Z^\bullet$ intermediate is only generated at illumination temperatures above 250 K (*13*, *17*, *18*, *20*). Thus, the upshift in the temperature of the S_1 to S_2 or S_2 to $S_2Y_Z^\bullet$ transitions in inhibited PSII samples also suggests that oxidation of Y_Z and/or oxidation of the Mn_4 cluster is impaired. While the concept that an intact Mn_4 cluster affects the properties of Y_Z is gaining ground (*28*, *64*), the idea that Y_Z exerts a significant impact on the properties of the Mn_4 cluster has not been previously considered in the context of the mechanism of water oxidation. Further experiments examining the importance of hydrogen bonding in the vicinity of Y_Z on the magnetic properties of the Mn_4 cluster and on the ability of Y_Z to be oxidized at low temperatures in O_2-evolving PSII will provide insight into proposed mechanisms of water oxidation.

ACKNOWLEDGMENT

We thank Dr. George Cheniae (University of Kentucky, Lexington, KY) for the generous gift of calcium-depleted and untreated PSII membranes and Dr. Mike Hendrich for assistance with parallel mode EPR measurements. We also thank Drs. Sandra and Gareth Eaton for helpful comments on the manuscript and Drs. R. David Britt, Richard Debus, and Gerald Babcock for providing manuscripts prior to publication.

REFERENCES

1. Ghanotakis, D. F., and Yocum, C. F. (1990) *Annu. Rev. Plant Physiol. Plant Mol. Biol. 41*, 255−276.
2. Debus, R. J. (1992) *Biochim. Biophys. Acta 1102*, 269−352.
3. Diner, B. A., and Babcock, G. T. (1996) in *Oxygenic Photosynthesis: The Light Reactions* (Ort, D., and Yocum, C., Eds.) pp 213−247, Kluwer Academic Publishers, Dordrecht, The Netherlands.
4. Kok, B., Forbush, B., and McGloin, M. (1970) *Photochem. Photobiol. 11*, 457−475.
5. Yachandra, V. K., DeRose, V. J., Latimer, M. J., Mukerji, I., Sauer, K., and Klein, M. P. (1993) *Science 260*, 675−679.
6. Miller, A.-F., and Brudvig, G. W. (1991) *Biochim. Biophys. Acta 1056*, 1−18.
7. Debus, R. J., Barry, B. A., Sithole, I., Babcock, G. T., and McIntosh, L. (1988) *Biochemistry 27*, 9071−9074.
8. Metz, J. G., Nixon, P. J., Rögner, M., Brudvig, G. W., and Diner, B. A. (1989) *Biochemistry 28*, 6960−6969.
9. Blankenship, R. E., Babcock, G. T., Warden, J. T., and Sauer, K. (1975) *FEBS Lett. 51*, 287−293.
10. Hoganson, C. W., and Babcock, G. T. (1988) *Biochemistry 27*, 5848−5855.
11. Tang, X.-S., Zheng, M., Chisholm, D. A., Dismukes, G. C., and Diner, B. A. (1996) *Biochemistry 35*, 1475−1484.
12. Boussac, A., and Rutherford, A. W. (1988) *Biochemistry 27*, 3476−3483.
13. Boussac, A., Zimmermann, J.-L., and Rutherford, A. W. (1989) *Biochemistry 28*, 8984−8989.
14. Sivaraja, M., Tso, J., and Dismukes, G. C. (1989) *Biochemistry 28*, 9459−9464.
15. Ono, T., and Inoue, Y. (1990) in *Current Research in Photosynthesis* (Baltscheffsky, M., Ed.) pp 741−744, Kluwer Academic Publishers, Dordrecht, The Netherlands.
16. Ono, T., and Inoue, Y. (1990) *Biochim. Biophys. Acta 1020*, 269−277.
17. Baumgarten, M., Philo, J. S., and Dismukes, G. C. (1990) *Biochemistry 29*, 10814−10822.
18. Andréasson, L.-E., and Lindberg, K. (1992) *Biochim. Biophys. Acta 1100*, 177−183.
19. MacLachlan, D. J., and Nugent, J. H. A. (1993) *Biochemistry 32*, 9772−9780.
20. Szalai, V. A., and Brudvig, G. W. (1996) *Biochemistry 35*, 1946−1953.
21. Gilchrist, M. L., Lorigan, G. A., and Britt, R. D. (1995) *Proc. Natl. Acad. Sci. U.S.A. 92*, 9545−9549.
22. Tang, X.-S., Randall, D. W., Force, D. A., Diner, B. A., and Britt, R. D. (1996) *J. Am. Chem. Soc. 118*, 7638−7639.
23. Szalai, V. A., and Brudvig, G. W. (1996) *Biochemistry 35*, 15080−15087.
24. Yocum, C. F., and Babcock, G. T. (1981) *FEBS Lett. 130*, 99−102.
25. Kalosaka, K., Beck, W. F., Brudvig, G. W., and Cheniae, G. (1990) in *Current Research in Photosynthesis* (Baltscheffsky, M., Ed.) pp 721−724, Kluwer Academic Publishers, Dordrecht, The Netherlands.
26. Lydakis-Simantiris, N., Dorlet, P., Ghanotakis, D. F., and Babcock, G. T. (1998) *Biochemistry 37*, 6427−6435.
27. Warden, J. T., Blankenship, R. E., and Sauer, K. (1976) *Biochim. Biophys. Acta 423*, 462−478.
28. Babcock, G. T., Espe, M., Hoganson, C., Lydakis-Simantiris, N., McCracken, J., Shi, W., Styring, S., Tommos, C., and Warncke, K. (1997) *Acta Chem. Scand. 51*, 533−540.
29. Hoganson, C. W., Lydakis-Simantiris, N., Tang, X.-S., Tommos, C., Warncke, K., Babcock, G. T., Diner, B. A., McCracken, J., and Styring, S. (1995) *Photosynth. Res. 46*, 177−184.
30. Hoganson, C. W., and Babcock, G. T. (1997) *Science 277*, 1953−1956.
31. Tommos, C., and Babcock, G. T. (1998) *Acc. Chem. Res. 31*, 18−25.
32. Lorigan, G. A., and Britt, R. D. (1994) *Biochemistry 33*, 12072−12076.
33. Berthold, D. A., Babcock, G. T., and Yocum, C. F. (1981) *FEBS Lett. 134*, 231−234.
34. Beck, W. F., de Paula, J. C., and Brudvig, G. W. (1985) *Biochemistry 24*, 3035−3043.
35. Arnon, D. I. (1949) *Plant Physiol. 24*, 1−15.
36. Tamura, N., and Cheniae, G. (1987) *Biochim. Biophys. Acta 890*, 179−194.
37. Beck, W. F., Innes, J. B., Lynch, J. B., and Brudvig, G. W. (1991) *J. Magn. Reson. 91*, 12−29.
38. Galli, C., Innes, J. B., Hirsh, D. J., and Brudvig, G. W. (1996) *J. Magn. Reson. 110B*, 284−287.
39. Force, D. A., Randall, D. W., and Britt, R. D. (1997) *Biochemistry 36*, 12062−12070.
40. Eaton, G. R., and Eaton, S. S. (1988) *Acc. Chem. Res. 21*, 107−113.
41. Lakshmi, K. V., Eaton, S. S., Eaton, G. R., Frank, H. A., and Brudvig, G. W. (1998) *J. Phys. Chem.* (in press).

42. Boussac, A., Zimmermann, J.-L., Rutherford, A. W., and Lavergne, J. (1990) *Nature 347*, 303−306.
43. Zimmermann, J.-L., Boussac, A., and Rutherford, A. W. (1993) *Biochemistry 32*, 4831−4841.
44. Koulougliotis, D., Tang, X.-S., Diner, B. A., and Brudvig, G. W. (1995) *Biochemistry 34*, 2850−2856.
45. Rupp, H., Rao, K. K., and Cammack, R. (1978) *Biochim. Biophys. Acta 537*, 255−269.
46. Hansson, Ö., Andréasson, L.-E., and Vänngård, T. (1984) in *Advances in Photosynthesis Research* (Sybesma, C., Ed.) pp 307−310, Nijhoff and Junk, The Hague, The Netherlands.
47. Hansson, Ö., Aasa, R., and Vänngård, T. (1987) *Biophys. J. 5*, 825−832.
48. Koulougliotis, D., Schweitzer, R. H., and Brudvig, G. W. (1997) *Biochemistry 36*, 9735−9746.
49. Boussac, A., and Rutherford, A. W. (1992) *Biochemistry 31*, 7441−7445.
50. Szalai, V. A., Kühne, H., Lakshmi, K. V., Eaton, G. R., Eaton, S. S., and Brudvig, G. W. (1998) *Biophys. J. 74*, A75.
51. Weil, J. A., Bolton, J. R., and Wertz, J. E. (1994) *Electron Paramagnetic Resonance Elementary Theory and Practical Applications*, John Wiley & Sons, Inc., New York.
52. Eaton, S. S., and Eaton, G. R. (1988) *Coord. Chem. Rev. 83*, 29−72.
53. Fielding, L., More, K. M., Eaton, G. R., and Eaton, S. S. (1986) *J. Am. Chem. Soc. 108*, 8194−8196.
54. Damoder, R., Klimov, V. V., and Dismukes, G. C. (1986) *Biochim. Biophys. Acta 848*, 378−391.
55. DeRose, V. J., Latimer, M. J., Zimmermann, J.-L., Mukerji, I., Yachandra, V. K., Sauer, K., and Klein, M. P. (1995) *Chem. Phys. 194*, 443−459.
56. Lindberg, K., and Andréasson, L.-E. (1996) *Biochemistry 35*, 14259−14267.
57. Boussac, A., Sétif, P., and Rutherford, A. W. (1992) *Biochemistry 31*, 1224−1234.
58. Hallahan, B. J., Nugent, J. H. A., Warden, J. T., and Evans, M. C. W. (1992) *Biochemistry 31*, 4562−4573.
59. Tommos, C., Tang, X.-S., Warncke, K., Hoganson, C. W., Styring, S., McCracken, J., Diner, B. A., and Babcock, G. T. (1995) *J. Am. Chem. Soc. 117*, 10325−10335.
60. Diner, B. A., Nixon, P. J., and Farchaus, J. W. (1991) *Curr. Opin. Struct. Biol. 1*, 546−554.
61. Hays, A.-M. A., Vassiliev, I. R., Golbeck, J. H., and Debus, R. J. (1998) *Biochemistry 37*, 11352−11365.
62. Nixon, P. J., and Diner, B. A. (1994) *Biochem. Soc. Trans. 22*, 338−343.
63. Roffey, R. A., Kramer, D. M., Govindjee, and Sayre, R. T. (1994) *Biochim. Biophys. Acta 1185*, 257−270.
64. Noguchi, T., Inoue, Y., and Tang, X.-S. (1997) *Biochemistry 36*, 14705−14711.
65. Casey, J. L., and Sauer, K. (1984) *Biochim. Biophys. Acta 767*, 21−28.
66. de Paula, J. C., Innes, J. B., and Brudvig, G. W. (1985) *Biochemistry 24*, 8114−8120.
67. Beck, W. F., de Paula, J. C., and Brudvig, G. W. (1986) *J. Am. Chem. Soc. 108*, 4018−4022.
68. Beck, W. F., and Brudvig, G. W. (1986) *Biochemistry 25*, 6479−6486.
69. Ono, T.-A., Zimmermann, J.-L., Inoue, Y., and Rutherford, A. W. (1986) *Biochim. Biophys. Acta 851*, 193−201.

BI9813025